# Design, Synthesis and Characterization of Nickel-Functionalized Covalent Organic Framework NiCl@RIO-12 for Heterogeneous Suzuki–Miyaura Catalysis

Renata A. Maia, Fabienne Berg, Vincent Ritleng, Benoit Louis, Pierre M. Esteves

# Design, Synthesis and Characterization of Nickel-Functionalized Covalent Organic Framework NiCl@RIO-12 for Heterogeneous Suzuki-Miyaura Catalysis

Renata A. Maia,[a,b] Fabienne Berg,[b] Vincent Ritleng,*[c,d] Benoît Louis,[b] and Pierre M. Esteves*[a]

**Abstract:** A series of nickel-decorated covalent organic frameworks, NiCl@RIO-12, were prepared using the Post-Synthetic Modification strategy, *i.e.*: by reacting $NiCl_2$ with pristine RIO-12 under alkaline conditions. Of interest, they retained their crystallinity and the amount of nickel incorporated was tuned from 3.6 to 25 wt% according to the reactions conditions. The incorporation of a higher amount of nickel in NiCl@RIO-12 consistently led to a lower BET surface area. Additionally, no agglomeration of nickel particles was found and a relatively homogeneous dispersion of nickel could be ascertained by SEM and TEM-EDS. The paramagnetic material exhibited promising catalytic activity in Suzuki-Miyaura cross-coupling under microwave heating. Thus, NiCl@RIO-12 notably demonstrated good thermal stability and its recyclability granted no substantial loss of activity upon 3 cycles.

## Introduction

Covalent Organic Frameworks (COFs)[1] represent a fascinating new type of crystalline porous organic materials, which are ingeniously constructed with organic building blocks *via* strong covalent bonds through the principles of reticular chemistry.[2–11] In comparison with Metal-Organic Frameworks (MOFs)[12,13] or their inorganic counterparts zeolites,[14,15] COFs stand out due to their low density,[4,16,17] large surface area,[8,16] good thermal stability,[16] tuneable pore size,[4,17] structure and functionality designability,[8,18] as well as to their versatile covalent-bonding of organic synthetic blocks,[19–23] consisting of light elements only.[1,10,17,24] These characteristics have offered the COF materials superior potential in various fields, such as gas storage,[17,25,26] adsorption,[4,27,28] optoelectronics,[29] energy storage[30] and conversion,[31] proton conduction,[32] drug delivery,[33–35] capacitance[36] and catalysis.[3,16] However, since Yaghi's landmark paper in 2005,[1] research in this field had been mainly focused on the design and synthesis of new COF structures intending to increase the surface area and pore volume.[16] For this reason, more recent studies concerning COFs applications have become a hot topic in organic chemistry.[37–40]

It can be highlighted that the first application in catalysis was only reported in 2011 by Ding *et al.*[2] with the robust incorporation of Pd(II) into the 2D imine-based scaffold LZU1 material. The resultant Pd/COF-LZU1 material was applied in Suzuki-Miyaura cross-coupling reactions. Excellent yields, high catalytic activity and easy recyclability have been achieved with Pd/COF-LZU1, but the exposure to harsh conditions and long reaction times diminished the structural regularity of the material. In 2016, Gonçalves *et al.*[24] reported that $Pd(OAc)_2$@COF-300 behaves as an effective heterogeneous catalyst with excellent catalytic activity for phosphine-free Suzuki-Miyaura, Heck and Sonogashira cross-coupling reactions at low palladium loadings (0.1 mol% Pd). In a similar fashion, Mu *et al.*[41] demonstrated that Cu-COFHX and Cu-COFDMF, both $Cu^{2+}$-containing COFs with imine linkers, exhibited high activities toward the selective oxidation of styrene to benzaldehyde. Additionally, Zhao *et al.*[42] displayed the synthesis of COF CPF-2, a porphyrinic framework, which showed high efficiency and selectivity for the aerobic epoxidation of alkenes under mild conditions after the coordination of $Co^{2+}$ ions.

So far, the construction of highly periodic and robust frameworks remains the greatest challenge in the synthesis of COF materials.[8,10] Nevertheless, suitable COF candidates for catalytic applications must show high stability to thermal treatments, water, and most organic solvents,[16] and should incorporate robust catalytic active sites.[2,41] Easy access to the latter and efficient mass transport within the porous catalyst should also be guaranteed for an ideal catalytic performance.[10] In contrast to the well-known boron-containing COFs linked by boroxine or boronate-ester groups, triazole-, imine-, and hydrazone-based COF materials present the stability characteristics stated previously and thus meet the requirements expected for robust heterogeneous catalysts.[2] Moreover, Schiff bases have played a central role as chelating ligands in coordination chemistry and are versatile in incorporating a variety of metal ions.[43,44]

This intrigued us to explore the possibility of using an imine-linked metal-ion-incorporated COF material for heterogeneous catalysis. In particular, we became interested in a microporous

[a] R. A. Maia, Prof. Dr. P. M. Esteves
Instituto de Química
Universidade Federal do Rio de Janeiro
Av. Athos da Silveira Ramos, 149, CT, Bl. A-622, Cid. Universitária, Ilha do Fundão, Rio de Janeiro, RJ, 21941-909, Brazil
E-mail: pesteves@iq.ufrj.br
[b] R. A. Maia, F. Berg, Dr. B. Louis
Université de Strasbourg, CNRS, ICPEES, UMR 7515
25 rue Becquerel, 67087 Strasbourg, France
[c] Prof. Dr. V. Ritleng
Université de Strasbourg, CNRS, LIMA, UMR 7042
25 rue Becquerel, 67087 Strasbourg, France
E-mail: vritleng@unistra.fr
[d] Prof. Dr. V. Ritleng
Institut Universitaire de France
1 rue Descartes, 75231 Paris, France.

Supporting information for this article is given via a link at the end of the document.

highly symmetrical azine-based COF, RIO-12,[8] prepared by the condensation of hydrazine hydrate and 1,3,5-triformylresorcinol. This material indeed presented itself as an ideal scaffold for catalysis, as the intramolecular hydrogen bonding led to higher symmetry of the framework, resulting in higher crystallinity and, consequently, higher surface area. Our strategy was to adopt a post-synthetic modification (PSM) of the potential catalytic sites into the COF skeleton to avoid the undesired effect of harsh solvothermal conditions.[22]

Despite the skyrocketing use of palladium in numerous catalytic systems over the past half-century, its high cost and relatively small earth abundance is a drawback when comparing it to other transition metals. Indeed, there is a trend to move towards greener chemistry by using more abundant, less toxic, non-precious and less expensive metal catalysts. In this context, Cifuentes *et al.*[18] recently described an iron-based covalent organic framework, $FeCl_3$@TPB-DMTP-COF, that can efficiently promote the decarboxylative cross-coupling of cinnamic acids. Likewise, nickel, the 3d sibling of palladium, outstands as an excellent choice when it comes to a more sustainable metal catalyst.[45–49] However, it should not be simply considered as an inexpensive alternative to palladium, but rather as an element presenting key properties that complement catalysis of other transition metals. Since nickel is a relatively electropositive transition metal, oxidative additions occur quite easily. Thus, the key advantage of Ni-based catalysts over Pd systems lies in their ability to activate aryl chlorides,[18] aryl fluorides,[46] sulfonates,[50] aromatic nitriles[46] and phenols derivatives[46] in cross-coupling reactions without the need of electron-rich and expensive ligands.[50] Nickel also has a wider range of oxidation states commonly invoked in catalysis. Even if Ni(0)/Ni(II) catalytic cycles are widespread, the easy accessibility of Ni(I) and Ni(III) oxidation states allows radical pathways, and thus different modes of reactivity. Additionally, nickel gains recognition because it is less susceptible to β -hydride-elimination relative to palladium.[46] In practical terms, the price of nickel in its elemental form is approximately 3,000 times lower than palladium, which now exceeds the price of gold on a kg-for-kg basis.

Concerning nickel anchored in COFs, research is still in its infancy. The first example of metalating a 3D COF with Ni was achieved by Baldwin *et al.*[51] by stirring DBA-3D-COF with 10 wt% $Ni(COD)_2$ in toluene. The resulting Ni-DBA-3D-COF displays great uptake capacities for ethane and ethylene. In 2016, the emergence of COFs as supports for electro-catalysts was revealed. Supporting $Ni_3N$ nanoparticles on a π-conjugated N-rich COF gave rise to lower band gap nanocomposites serving as excellent electro-catalysts for oxygen evolution reaction (OER) from water.[52] Shortly afterwards, covalent triazine frameworks with 2.8 wt% Ni loadings were applied as catalysts in the oligomerization of ethylene under mild conditions (15 bar at 50°C). These porous aromatic frameworks exhibited similar catalytic activities compared to those of their homogeneous analogues and a fivefold higher selectivity to long-chain olefins $C_{6+}$. Recently, Dong *et al.* reported outstanding photocatalytic activity for $H_2$ production by a visible-light active nickel hydroxide-modified COF (TpPa-2).[53]

Encouraged by these promising results of nickel-based COF catalysts, we turned our attention on exploring the COF RIO-12 topology for nickel-catalysed Suzuki-Miyaura aryl-aryl cross-coupling, a powerful tool to construct C-C bonds[50,54] and a relevant reaction for the synthesis of several drugs. The nickel(II)-coordinated COF material (denoted NiCl@RIO-12) was easily synthesized by refluxing RIO-12 with $NiCl_2$ in ethanol in the presence of $K_2CO_3$. Ni(II)-incorporation in the resulting NiCl@RIO-12 was verified by X-ray photoelectron spectroscopy (XPS), and a homogeneous Ni-dispersion throughout the framework was established by scanning electron microscopy (SEM) and high resolution transmission electron microscopy (HRTEM), both coupled with energy dispersive X-ray spectrometry (EDS). The designed material NiCl@RIO-12 was applied as a heterogeneous catalyst for Suzuki-Miyaura reactions under microwave conditions between 4'-bromoacetophenone and phenylboronic acid with nickel loadings as low as 0.2 mol%. Conversions to the cross-coupled product were moderate, but these results are promising as, to the best of our knowledge, there are no reports of microwave heating to heterogeneous catalysis using a nickel-functionalized COF.

## Results and Discussion

### Synthesis and characterization of the model compound $NiL_n$@SA

RIO-12 is a microporous COF with a high surface area, which synthesis is based on the condensation reaction of a hydroxylated triformylbenzene moiety with hydrazine hydrate.[8] In order to investigate and optimize the complexation reaction of the nickel into the framework of RIO-12, a model compound approach was employed. The use of a small molecule that can closely represent the chemical structure of the framework, in theory, indeed allows the rapid characterization of the resulting complex by solution NMR spectroscopy and other conventional techniques, in spite of the time-consuming characterization of COFs and related materials. Considering the structure of RIO-12, a α-imine-phenol moiety was the obvious choice for the model compound (Figure 1), and the synthetic equivalent, salicylideneaniline (SAH), was thus chosen, due to the readily available starting materials: salicylaldehyde and aniline. On that basis, SAH was reacted with nickel dichloride in order to afford $NiL_n$@SA, and an optimization study was conducted concerning the base and the solvent. The optimized conditions were then employed on RIO-12 to afford the product NiCl@RIO-12.

The various reaction conditions used to obtain a model complex $NiL_n$@SA are summarized in Table 1. The model compound salicylideneaniline (SAH) was initially reacted with the anhydrous nickel salt in methanol at 65 °C.[44] However, only the starting material was detected by $^1$H NMR spectroscopy of the reaction medium after 24 h reaction (entry 1). In contrast, when 0.5 or 1.0 equivalent of potassium carbonate was used (entry 2 and 3) a light green solid was obtained after filtration of the reaction medium with 23 or 79% estimated yield, assuming that a 1:1 complexation had occurred. This showed that the

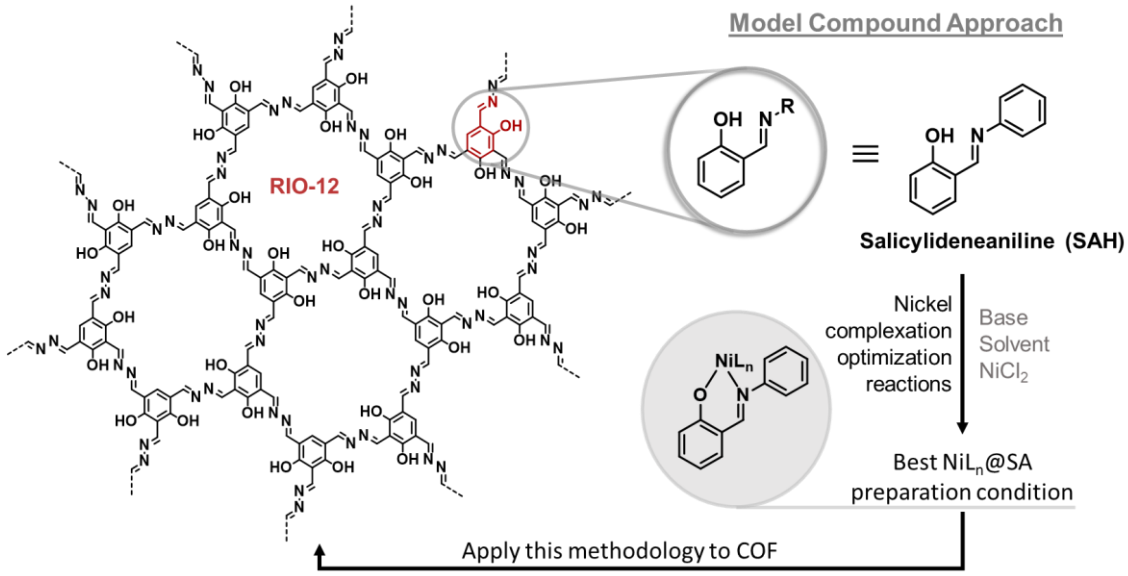


**Figure 1.** Chemical structure of RIO-12 (left) and representation of the model compound approach (right)

deprotonation of the phenol moiety is necessary to enable the complex formation, even though similar complexations have been reported to occur without a base.[55–57] Bearing entry 2 as the best result in methanol, the screening of different reaction solvents was next performed.

Regarding this latter point, it is noteworthy that, since the optimized reaction conditions will be used in a COF, solvent surface tension must be taken into account. The porosity of the COF can only be accessed if the solvent in which the material was held in is adequately removed; usually under high vacuum

**Table 1.** Optimization of nickel complexation with salicylideneaniline (SA) to obtain $NiL_n$@SA.

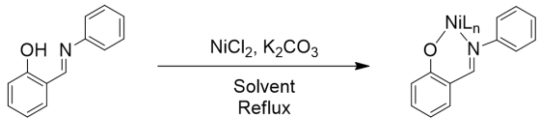


**SAH** **$NiL_n$@SA**

| Entry | Solvent | $K_2CO_3$ (equiv.) | Temp. (°C) | Time (h) | Estimated Yield (%)[a] |
|---|---|---|---|---|---|
| 1 | MeOH | 0 | 65 | 24 | 0 |
| 2 | MeOH | 0.5 | 65 | 24 | 23 |
| 3 | MeOH | 1.0 | 65 | 24 | 79 |
| 4 | Toluene | 1.0 | 110 | 15.5 | 0 |
| 5 | THF | 1.0 | 66 | 24 | 57 |
| 6 | $CH_2Cl_2$ | 1.0 | 40 | 24 | 46 |
| 7 | EtOH | 1.0 | 78 | 24 | 89 |

[a] The yields were estimated considering a hypothetical $K[Ni(SA)Cl_2]$ ($C_{13}H_{10}Cl_2KNiO$) formula of the product.

at room (or higher) temperature. However, a solvent with a high surface tension will adhere by capillarity to the pore walls and will either (i) be trapped into the pores or (ii) collapse the framework due to structural deformation during solvent evacuation.[58] For that matter, solvents with a high surface tension such as DMSO (42.9 dynes/cm) were avoided, and solvents with a milder surface tension (22-28 dynes/cm), such as methanol, ethanol, toluene, THF and dichloromethane were preferred.[59]

When the reaction was performed in toluene (entry 4), the reaction presented itself as a suspension at all times and no product was formed. In contrast, when the reaction was performed in THF (entry 5) and $CH_2Cl_2$ (entry 6), moderate yields, of 57% and 46% were obtained. Finally, when the reaction was held in ethanol (entry 7), the estimated yield was 89%. The latter was thus chosen as the reaction solvent.

HRMS-ESI analysis of $NiL_n$@SA confirmed nickel complexation by the detection of a mixture, comprising $[Ni(SA)(NCMe)(OH_2)]^+$, $[Ni(SA)_2]^+$, and the $[Ni_2(SA)_3]^+$ oligomer (Figures S1-S4). In agreement with these data, the infrared spectrum of $NiL_n$@SA differs from that of starting material SAH, most notably by the change of the C=N vibration to a lower wavenumber, shifting from 1613 $cm^{-1}$ to 1606 $cm^{-1}$ as a result of the weakening of the imine bond, and by the shift of the phenolic C-O vibration band at 1273 $cm^{-1}$ to 1308 $cm^{-1}$ due to metal complexation[60,61] (Figure S5).

The characterization of $NiL_n$@SA was not possible by $^1H$ or $^{13}C$ NMR spectroscopy due to the paramagnetic behavior of the complex. XPS analysis of $NiL_n$@SA was thus carried out. The XPS spectra of the Ni 2p and Cl 2p regions of $NiL_n$@SA are shown in Figure 2a,b and the binding energies (BE) are detailed in Table 2. The presence of the $2p_{3/2}$, $2p_{1/2}$ peaks and their respective satellites confirms that the nickel compound is paramagnetic. Based on the Russell-Saunders selection rules for nickel compounds, the spin-orbit coupling is forbidden in

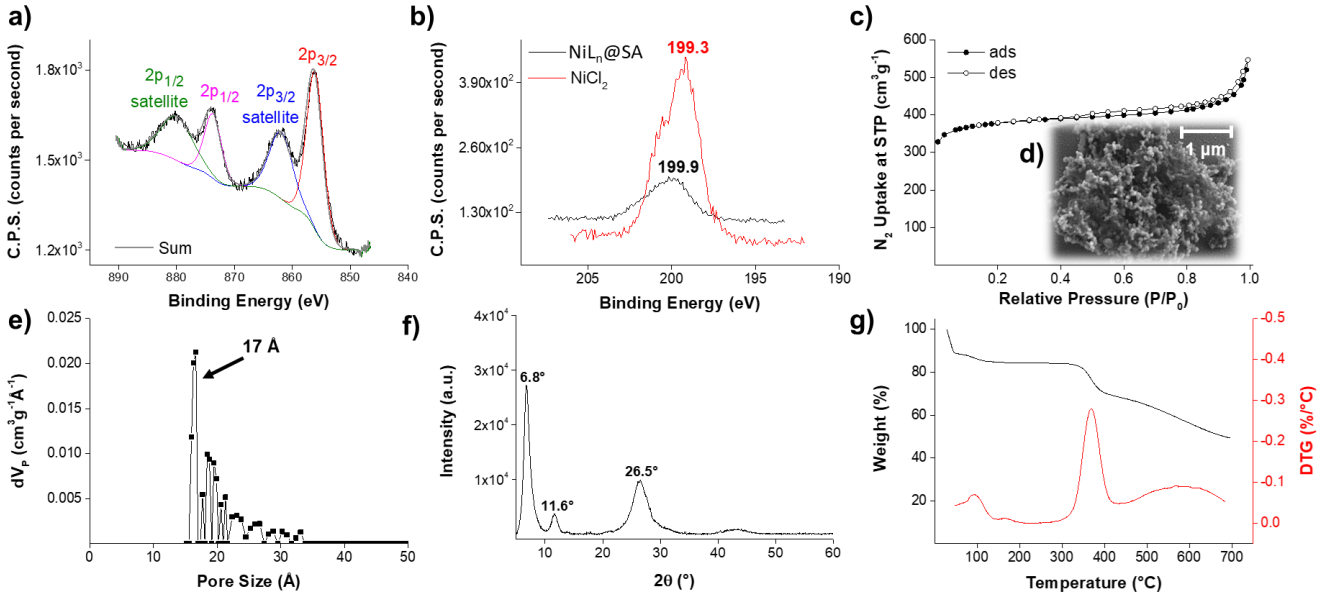


**Figure 2.** XPS spectra for the nickel 2p region (a) and for the chlorine 2p region (b) of $NiL_n$@SA; $N_2$ adsorption-desorption isotherm at 77 K (c), SEM micrograph, (d) Pore size distribution, (e) PXRD profile (f) and TGA measurement under $N_2$ flow (g) of RIO-12.

**Table 2.** XPS binding energies (BE) for the nickel 2p peaks and their satellites (sat.).

| Compound | $2p_{3/2}$ (eV) | Sat. $2p_{3/2}$ (eV) | $2p_{1/2}$ (eV) | Sat. $2p_{1/2}$ (eV) |
|---|---|---|---|---|
| $NiCl_2$ | 855.3 | 860.9 | 872.6 | 878.4 |
| $NiL_n$@SA | 856.0 | 861.9 | 873.1 | 879.9 |

diamagnetic compounds, but it is allowed in paramagnetic compounds, which leads to the transition BE associated with these satellites. This allowed transition is related to the shake-up transition between 3d and 4s orbitals.[62] Furthermore, the similar BE of the 2p peaks and their satellites for $NiCl_2$ and $NiL_n$@SA clearly indicate a $Ni^{2+}$ species (Table 2).[63] Finally, the presence of a nickel-bonded chlorine atom in the $NiL_n$@SA can be justified by the characteristic Ni-Cl BE for this atom (Figure 2b). On these bases, a $K[Ni(SA)Cl_2]$ or $[Ni(SA)Cl(L)]$ (where L = solvent or $H_2O$) formulation can reasonably be proposed for the monomeric form of our model compound $NiL_n$@SA. Unfortunately, elemental analyses could not confirm either of these formulations and no single crystals could be obtained to confirm (or infirm) this hypothesis by X-ray diffraction crystallography, most probably because of the presence of dimeric and oligomeric forms, as shown by HRMS.

Having these optimized conditions in hand for the complexation of $NiCl_2$ by SAH, and in mind that dimers and oligomers cannot form with RIO-12, this methodology was then applied to the latter to afford the nickel-functionalized COF materials NiCl@RIO-12.

### Synthesis and characterization of NiCl@RIO-12 materials

Firstly, RIO-12 was prepared by a condensation reaction of 1,3,5-triformylresorcinol and hydrazine hydrate 60%.[8] The starting materials were added in a Chemglass® high-pressure vessel in a mixture of mesitylene/dioxane 1:11, followed by the addition of acetic acid 6 M. The vessel was sealed and the mixture was reacted at 120 °C for 72 h. The resulting red powder, which is insoluble in most common solvents, was filtered off and washed thoroughly with MeOH, DMF and THF to remove the starting materials and soluble oligomers. Afterward, the product was soaked in THF for 72 h at room temperature to unclutter the pores and filtered off again. The resulting red powder was dried under vacuum and characterized by $N_2$ adsorption-desorption isotherm, scanning electron microscopy (SEM), powder X-Ray diffraction (PXRD), thermogravimetric analysis (TGA) and infrared spectroscopy (IR).

The textural properties were measured by $N_2$ adsorption-desorption isotherm at 77 K and SEM. The Brunauer-Emmett-Teller (BET) linearized equation was employed to access the surface area ($S_{BET}$) and pore size was determined by the Non-Local Density Functional Theory (NLDFT). RIO-12 exhibited a type I isotherm (Figure 2c), typical of microporous materials according to the IUPAC classification.[64] RIO-12 presented $S_{BET}$ of 1458 $m^2/g$, which basically corresponds to 100% of the $S_{BET}$ derived theoretically (1471 $m^2/g$).[8] Furthermore, the t-Plot analysis revealed that 1210 $m^2/g$ is related to the micropore surface area ($S_{Micro}$) and 248 $m^2/g$ is related to the external surface area ($S_{Ext}$) with a micropore volume of 0.48 $cm^3/g$. The pore size distribution analysis from gas adsorption isotherm for RIO-12 indicates pores of 17 Å or smaller (Figure 2e). Additionally, SEM images revealed a coral-like morphology, consisting of agglomerated/sintered particles (Figure 2d).

Powder XRD of RIO-12 (Figure 2f) showed a crystalline material with diffraction peaks at 6.8°, 11.6° and 26.5° corresponding to the lattice planes (100), (210) and (002), respectively.[8] The broad peak at 26.5° is attributed to π-stacking of the 2D sheets[65] with an interplanar distance of 3.4 Å,

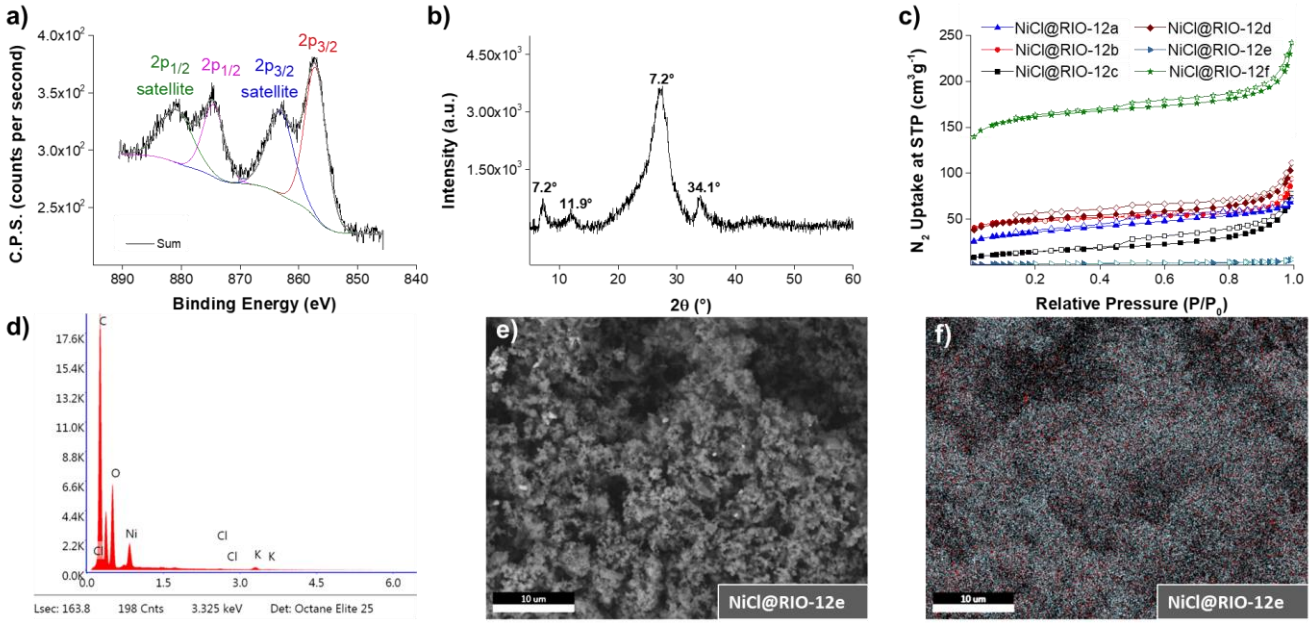


**Figure 3.** (a) XPS and (b) powder X-ray diffraction spectra of NiCl@RIO-12**e**; (c) $N_2$ adsorption-desorption isotherms for NiCl@RIO-12**a-f** materials; closed and open symbols for adsorption and desorption, respectively. (d) EDS spectrum, (e) SEM micrograph and (f) Nickel mapping (in red) by SEM-EDS for NiCl@RIO-12**e.**

compatible with graphite interlayer distance.[66,67] RIO-12 showed a mean crystalline domain of 7.0 nm, determined by Scherrer's equation,[68] when the spherical shape factor of 0.9 was employed.

The thermal stability of RIO-12 was determined by TGA under $N_2$ flow (Figure 2g). The mass loss up to 66°C is attributed to THF within the pores. It corresponds to 2 molecules per pore of a COF single layer. The discrete weight change seen at 100°C is also attributed to solvent loss. Further heating did not lead to weight loss up to 370°C, demonstrating the excellent thermal stability of the material.

Finally, RIO-12 was also characterized by IR spectroscopy. The IR spectrum (Figure S6) shows the stretching modes of the C=N bonds at 1591 $cm^{-1}$ and of the aromatic C-H bonds at 2975 $cm^{-1}$. The residual Fermi resonance peak observed at 2860 $cm^{-1}$ in RIO-12 can be attributed to terminal aldehyde moieties present in the framework.

The optimized conditions used to prepare $NiL_n$@SA (Table 1, entry 7) were then applied to RIO-12 to afford NiCl@RIO-12. RIO-12 was thus refluxed with $K_2CO_3$ (2.0 equiv. per periodic unit) and different amounts of anhydrous $NiCl_2$ in dry ethanol for 24 h to give a series of NiCl@RIO-12**a-f** materials. The resulting dark purple powders were filtered off, washed with degassed water and ethanol and dried under vacuum. Table 3 summarizes the obtained results for the $S_{BET}$, pore volume and nickel quantification.

The tunability of nickel incorporation into RIO-12 was remarkable. The amount of nickel analysed in the framework by inductively coupled plasma–atomic emission spectroscopy (ICP-AES) ranged from 3.6 wt% to 25 wt% in NiCl@RIO-12**a-f** (Table 3), depending on the amount of nickel salt used in its synthesis (from 0.2 to 30 equiv. per periodic unit). And the higher the amount of nickel, the more potential chelating sites of pristine RIO-12 – present within the pores – are occupied by the metal and its ligands. Thus, at the exception of NiCl@RIO-12**c** and NiCl@RIO-12**e**, which surfaces may not be accessible by $N_2$ sorption measurements, a higher metal content consistently led to a lower surface area and pore volume of the resulting material.

**Table 3.** Quantification of nickel, surface area, pore volume and pore size for NiCl@RIO-12**a-f**.[a]

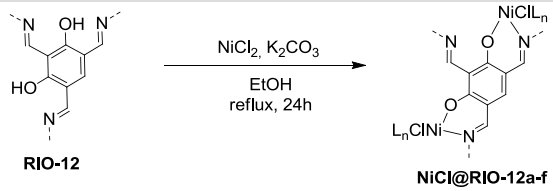


| Entry | NiCl@ RIO-12 | $NiCl_2$ (equiv.)[b] | %Ni (wt%) | $S_{BET}$ ($m^2$/g) | $S_{Micro}$ ($m^2$/g) | $V_{Micro}$ ($cm^3$/g) |
|---|---|---|---|---|---|---|
| 1 | **a** | 30 | 25 ± 1.0 | 128 | 48 | 0.0204 |
| 2 | **b** | 10 | 17 ± 0.5 | 186 | 134 | 0.0533 |
| 3 | **c** | 2 | 14.2 ± 0.4 | 43 | *[c] | * |
| 4 | **d** | 1 | 12.0 ± 0.3 | 182 | 99 | 0.0405 |
| 5 | **e** | 0.5 | 7.0 ± 0.2 | 88 | * | * |
| 6 | **f** | 0.2 | 3.6 ± 0.8 | 616 | 488 | 0.1925 |

[a] Reactions conditions: RIO-12 (1 equiv., 0.37 mmol of periodic unit, 70 mg), $K_2CO_3$ (same number of equiv. as $NiCl_2$) and $NiCl_2$ in dry ethanol (15 mL) at reflux for 24 h. [b] Number of equivalents per periodic unit. [c] *Not accessible by $N_2$.

A type I isotherm was confirmed for all as-prepared materials (Figure 3c). In addition, SEM images of NiCl@RIO-12**a-f** samples revealed a coral-like morphology similar to that of the parent material RIO-12 for all Ni-functionalized COFs (see Figure 3e for NiCl@RIO-12**e** and Figure S7 for NiCl@RIO-12**a-f** materials).

Elemental mapping of the nanostructure was performed by SEM-EDS to access the chemical composition of the sample. The EDS spectrum of NiCl@RIO-12**e** (Figure 3d) reveals the presence of nickel in the material, whereas the elemental representation of nickel (red) in the SEM (Figure 3f) showed no apparent agglomeration of the metal in the material. In addition, TEM-EDS mapping was performed for samples NiCl@RIO-12**c** (14 wt% Ni) and NiCl@RIO-12**f** (3.6 wt% Ni) in order to further evaluate the dispersion of nickel atoms in samples with higher and lower content of nickel (Figure 4 and S8). Carbon, nitrogen and oxygen are present in both samples due to the chemical nature of the organic framework (Figure S8). Furthermore, the nickel atoms are well dispersed in both materials (Figure 4), showing that, during the synthesis, the reagents show good diffusivity through the nanopore channels of RIO-12, hence promoting a homogeneous distribution of nickel within the framework. This absence of agglomeration of nickel also indicates that no sintering occurred during the synthesis of these NiCl@RIO-12 compounds.

The XPS spectrum of NiCl@RIO-12**e** revealed a paramagnetic material (Fig. 3a) resembling the model compound, $NiL_n$@SA. The peaks values for $2p_{3/2}$, $2p_{3/2}$ satellite, $2p_{1/2}$ and $2p_{1/2}$ satellite of the 2p nickel region are found at 857.2, 863.1, 874.5 and 880.8 eV, respectively. These values are consistent with an oxidation state of $Ni^{2+}$. Furthermore, powder XRD of NiCl@RIO-12**e** confirms that the material remains crystalline after nickel incorporation (Figure 3b). The diffraction 2θ peaks of at 7.2°, 11.9°, 27.5° and 34.1° are slightly shifted to higher 2θ angles when compared to the pristine material. This indicates a small contraction of the unit cell. The interlayer distance of the 2D layers of the material was found to be 3.2 Å

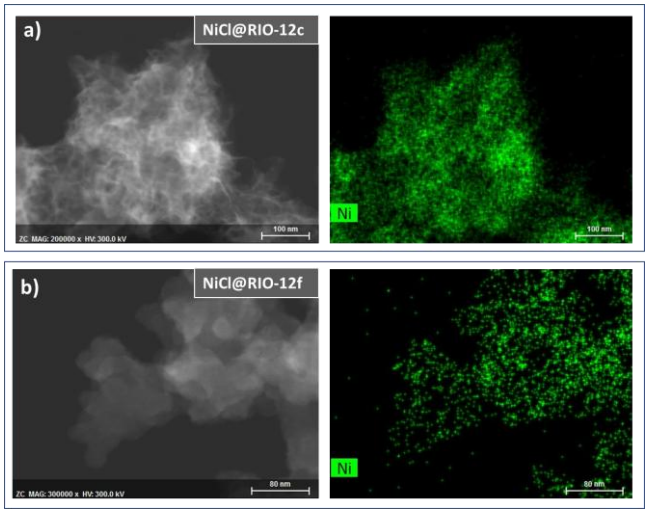


**Figure 4.** TEM-EDS mapping of Ni, C, O and N elements for NiCl@RIO-12**c** (a) and NiCl@RIO-12**f** (b).

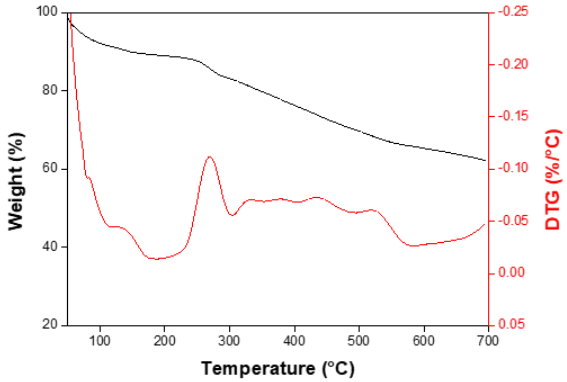


**Figure 5.** TGA measurement under $N_2$ flow for NiCl@RIO-12**e**.

according to Bragg's law, which brings to the conclusion that the presence of nickel in the framework holds the COF sheets slightly closer together. Furthermore, the mean crystalline domain determined by the Scherrer method also increased to 9.5 nm when compared to the parent material (7.0 nm). Finally, the material was analyzed by TGA under $N_2$ flow, NiCl@RIO-12**e** presented good thermal stability up to 270°C (Figure 5), but when comparing NiCl@RIO-12**e** to the pristine material, the former was less stable towards heating than the latter, since the decomposition temperature of RIO-12 was 370°C.

## Catalytic studies

The obtained NiCl@RIO-12**a-f** materials were then tested as potential heterogeneous catalysts in a Suzuki-Miyaura cross-coupling reaction between 4'-bromoacetophenone (1.0 equiv.) and phenylboronic acid (1.3 equiv.), employing tripotassium phosphate as a base (2.6 equiv.), and toluene as the reaction solvent.[69] Initially, 10 mol% NiCl@RIO-12**a** (Table 4, entry 1) or NiCl@RIO-12**b** (entry 2) were employed in a conventional thermal coupling attempt, *i.e.*: in toluene at reflux. In both cases, no product was detected after 24 h reaction and only unreacted starting materials were recovered.

Based on recent advances in employing nickel catalysts for Suzuki-Miyaura reactions,[45,70] and considering the benefit of lowering the reaction time as well as that of an energy-efficient heating, microwave radiation was employed for our next trials. However, when 10 mol% of NiCl@RIO-12**a** was employed using microwave radiation (180°C, 2.45 GHz) for 15 min (entry 3) or 60 min (entry 4), no product could be observed either. Similarly when NiCl@RIO-12**b** was used under the same conditions, no product was detected after 15 min (entry 5). However, when the same catalyst was employed for 60 min, 12% conversion to 4-acetylbiphenyl was achieved (entry 6). The other NiCl@RIO-12 materials were then also screened under microwave irradiation. NiCl@RIO-12**c** and NiCl@RIO-12**d** (10 mol%) gave 7% and 10% of conversion after 15 min irradiation (entries 7 and 8). When the amount of NiCl@RIO-12**d** was decreased to 1 mol% (entry 9), the conversion dropped to almost none after 15 min. In contrast, when 1 mol% of NiCl@RIO-12**e** (entry 10) or NiCl@RIO-12**f** (entry 11) was used, the conversions were of 7%

**Table 4.** Suzuki-Miyaura cross-coupling reaction employing NiCl@RIO-12**a-f** and $NiL_n$@SA as the catalyst.

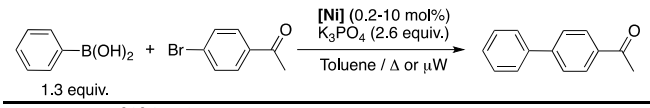


1.3 equiv.

| Entry | NiCl@RIO-12a-f or $NiL_n$@SA (mol%) | Heating cond.[a,b] | T (°C) | Time (min) | Conv. (%)[c] |
|---|---|---|---|---|---|
| 1 | **a** (10) | Conventional | 110 | 1440 (24 h) | 0 |
| 2 | **b** (10) | Conventional | 110 | 1440 (24 h) | 0 |
| 3 | **a** (10) | MW | 180 | 15 | 0 |
| 4 | **a** (10) | MW | 180 | 60 | 0 |
| 5 | **b** (10) | MW | 180 | 15 | 0 |
| 6 | **b** (10) | MW | 180 | 60 | 12 |
| 7 | **c** (10) | MW | 180 | 15 | 7 |
| 8 | **d** (10) | MW | 180 | 15 | 10 |
| 9 | **d** (1) | MW | 180 | 15 | traces |
| 10 | **e** (1) | MW | 180 | 15 | 7 |
| 11 | **f** (1) | MW | 180 | 15 | 9 |
| 12 | **f** (1) | MW | 180 | 60 | 9 |
| 13[d] | **f** (3) | MW | 180 | 60 | 6 |
| 14 | **e** (0.2) | MW, GB | 180 | 15 | 34 |
| 15 | **e** (0.2) | MW, GB | 180 | 60 | 34 |
| 16 | **f** (0.2) | MW, GB | 180 | 15 | 14 |
| 17 | $NiL_n$@SA (0.2) | MW, GB | 180 | 15 | 9 |

[a] MW = Microwave. [b] GB = Glovebox. [c] Conversion to 4-acetylbiphenyl was determined by $^1$H NMR; no homocoupling was observed, and only the starting materials were detected in addition to the cross-coupling product. [d] Reaction run with 4'-iodoacetophenone instead of 4'-bromoacetophenone.

and 9% after 15 min, respectively. Running the reaction for 60 min with the latter (entry 12) did however not improve the conversion, suggesting either a fast catalyst deactivation or a diffusion issue due to pore blocking by the reaction product. Additionally, using a higher NiCl@RIO-12**f** content (3 mol%) and running the reaction with 4'-iodoacetophenone as the aryl halide did not result in a better conversion (entry 13). Taking into consideration the possible air and moisture sensitivity of these nickel-based catalysts, a reaction using 0.2 mol% of NiCl@RIO-12**e** was set up in a glovebox, which granted argon atmosphere and a moisture-free environment. For that purpose, the dry reagents and the degassed and dry solvent were added in a microwave vial inside the glovebox, the vial was tightly sealed and immediately placed in a microwave reactor. Satisfyingly, a conversion of 34% was observed after 15 min reaction (entry 14). Increasing the reaction time to 60 min unfortunately resulted in no further gain (entry 15), similarly to what had been observed with NiCl@RIO-12**f** (entries 11 and 12). Finally, considering the much higher surface area and pore volume of NiCl@RIO-12**f**, the latter was also tested after preparation of the vial in a glovebox, but the conversion was only 14% after 15 min of reaction (entry 16).

The recyclability of NiCl@RIO-12**e** was next investigated under the conditions of Table 4, entry 13. After the reaction was over, the catalyst was recovered by filtration, washed with ethanol and dried under reduced pressure. The so recovered catalyst was used in three consecutive catalytic runs. Conversions of 34%, 32% and 26%, were observed after the first, second and third cycles, respectively, showing the recyclability of our catalytic COF. Importantly, despite the slight decrease in activity observed for the 3$^{rd}$ run, a hot filtration test carried out with a fresh sample of NiCl@RIO-12**e** revealed no nickel leaching into the solution (see experimental section), therefore confirming the heterogeneous nature of the catalyst.

Finally, in view of benchmarking NiCl@RIO-12**e** with the homogeneous catalyst $NiL_n$@SA, a reaction was performed employing the reaction conditions of Table 4, entry 14 with the latter. When 0.2 mol% of $NiL_n$@SA was employed, only 9% of product conversion was observed after 15 min reaction (Table 4, entry 17), perhaps in reason of the presence of dimers or oligomers, which may lower its activity. Anyhow, this shows the superiority of the nickel-functionalized COF under such conditions.

## Conclusions

In this work, we have synthetized a nickel-functionalized COF, NiCl@RIO-12, based on a model compound approach. The model molecule, salicylideneaniline (SAH), was reacted with $NiCl_2$ in the presence of 1.0 equivalent of $K_2CO_3$ in ethanol at reflux to afford the desired complex $NiL_n$@SA. Similar reaction conditions were used to incorporate nickel in various amounts in the framework of RIO-12. The resulting nickel-decorated COFs preserved their crystallinity, as shown by powder XRD, and higher loadings of nickel in general led to lower BET surface areas. Moreover, the incorporation of nickel was relatively homogeneous and no agglomeration was detected by SEM-EDS or HRTEM-EDS. Furthermore, the paramagnetic nature of NiCl@RIO-12**a-f** was established by XPS. NiCl@RIO-12**e** was applied in Suzuki-Miyaura cross-coupling reactions under microwave radiation for 15 minutes. Though its catalytic activity was moderate, it was recyclable and showed no nickel leaching, which makes of it a superior catalyst than the homogeneous model catalyst.

Considering that nickel-functionalized COFs are still in their infancy,[50–53] as well as the importance of employing earth abundant metals over precious metals as catalysts, we expect that this work will highlight that nickel-functionalized COFs have the potential of being employed in heterogeneous catalysis. The stable nickel-COF bond, its homogeneous dispersion throughout the framework, its recyclability and the absence of leaching are factors that make this kind of material promising for a variety of

applications in catalysis, and we expect a bright future for Ni@COF materials.

## Experimental Section

*Materials and Methods*

All solvents were purified and dried by standard literature procedure prior to use. Unless otherwise stated, all reactions were performed in oven-dried or flame-dried glassware with magnetic stirring under an atmosphere of dry argon. Solution NMR spectra were recorded at 298 K on a Bruker Spectrospin 400 spectrometer operating at 400.13 MHz, the chemical shifts are referenced to the residual deuterated or $^{13}C$ solvent peaks. IR spectra were recorded on a Perkin Elmer Spectrum Two spectrometer. HRMS were recorded on a Bruker micrOTOF-Q mass spectrometer by the Laboratoire de Spectrométrie de Masse BioOrganique, IPHC (UMR CNRS 7178), Université de Strasbourg. X-ray photoelectron (XPS) spectra were acquired on a Thermo Fischer ThermoVGMultilabESCA3000 under ultra-high vacuum, the baseline was subtracted from the spectra, calibration was performed by adventitious carbon at 284.8 eV and data were analyzed by CASAXPS version 2.3.15 software. Brunauer – Emmett – Teller surface areas ($S_{BET}$) nitrogen adsorption-desorption isotherms were measured at 77 K by a Micromeritics ASAP2420, the samples were held overnight at 120°C under vacuum prior to analysis. PXRD patterns were recorded on a Bruker D8 Advance diffractometer with a Cu $K_\alpha$ wavelength. TGA was performed using TA Instruments Q5000IR in $N_2$ atmosphere. ICP-AES measurements were performed by the Plateforme Analytique, IPHC (UMR CNRS 7178), Université de Strasbourg, France. SEM micrographs were obtained with a Zeiss GeminiSEM 500 microscope with a FEG Schottky source and an Everhart-Thornley detector. The microwave reactions were performed in a Discover CEM S-class microwave operating at 2.45 GHz. Commercially available reagents were used as received. Salicylideneaniline (SAH) was prepared according to the literature procedure.[71]

*Synthesis of $NiL_n$@SA*

In a two-neck round bottom flask, equipped with a condenser and stirring bar, were added salicylideneaniline (SAH) (1 equiv., 2 mmol, 0.396 g), $K_2CO_3$ (1 equiv., 2 mmol, 0.279 g) and anhydrous $NiCl_2$ (1 equiv., 2 mmol, 0.265). After the addition of dry ethanol (50 mL), the mixture was refluxed for 24 h with continuous stirring and then allowed to cool slowly to room temperature. The resulting green precipitate was filtered off in a Büchner funnel and washed thoroughly with anhydrous ethanol (*ca.* 100 mL) and dried under vacuum to afford the light green powder $NiL_n$@SA (0.324 g, 89% $K[Ni(SA)Cl_2]$ ($C_{13}H_{10}Cl_2KNiO$) formulation). DRIFTS-FTIR: v ($cm^{-1}$): 1606 (C=N), 1308 (C-O). HRMS-ESI (MeCN): *m/z* $[M]^+$ calcd. for $[Ni(SA)(NCMe)(OH_2)]^+$ ($C_{15}H_{15}N_2NiO_2$) 313.0481, found 313.0484; calcd. for $[Ni(SA)_2+H]^+$ ($C_{26}H_{20}N_2NiO_2$) 451.0951, found 451.0952; calcd. for $[Ni_2(SA)_3]^+$ ($(C_{13}H_{10}NO)_3Ni_2$) 704.0989, found 704.0982.

*Synthesis of RIO-12*

To a high-pressure vessel of 48 mL, it was added 1,3,5-triformylresorcinol (1 equiv., 3 mmol, 0.582 g), freshly distilled dioxane (20 mL) and mesitylene (1.8 mL). Hydrazine 60% (1.5 equiv., 4.5 mmol, 0.25 mL) was added to the yellow suspension, which immediately turned red. Acetic acid 6 M (7 mL) was then added and the reaction was held at 120 °C for 72 h. The resulting solid was filtered off in a Büchner funnel and sequentially washed thoroughly with MeOH, DMF and THF (portions of 100 mL), followed by soaking the powder in THF for three days to unclutter the pores. The resulting material was collected by filtration, washed with THF and dried under vacuum to give RIO-12, a red powder (0.587 g, >99%).

*Synthesis of NiCl@RIO-12*

In a two-neck round bottom flask, equipped with a condenser and stirring bar, was added RIO-12 (1 equiv., 0.37 mmol of periodic unit, 70 mg), $K_2CO_3$ (same number of equiv. as $NiCl_2$) and $NiCl_2$ (0.2 to 30 equiv., 0.074 mol to 11.1 mmol, see Table 3) and dry ethanol (15 mL). The reaction was refluxed for 24 h. The mixture was then allowed to cool to room temperature and the dark purple solid was filtered off, and washed thoroughly with dry ethanol and dried under vacuum.

*General procedure for the Suzuki-Miyaura cross-coupling reactions*

Conventional procedure: A Schlenk tube was charged with 4'-bromoacetophenone (1 equiv., 1 mmol, 0.203 g), phenylboronic acid (1.3 equiv.,1.3 mmol, 0.162 g), tripotassium phosphate (2.6 equiv., 2.6 mmol, 0.563 g) and the catalyst. Freshly distilled toluene (3 mL) was added via syringe and the suspension was stirred under reflux for 24 h. An aliquot was then removed with a syringe, dried under vacuum and the residue was dissolved in $CDCl_3$ and filtered off into an NMR tube.
Microwave procedure: A 10 mL microwave vial containing a stirring bar was charged with 4'-bromoacetophenone (1 equiv., 1 mmol, 0.203 g), phenylboronic acid (1.3 equiv.,1.3 mmol, 0.162 g), tripotassium phosphate (2.6 equiv., 2.6 mmol, 0.563 g), the catalyst and dry toluene (3 mL). The mixture was placed in a microwave reactor and it was pre-mixed at room temperature for 30 seconds. After that, the reaction was heated at 180°C for the appropriate time. After the reaction time was over, an aliquot was removed with a syringe, dried under vacuum and the residue was dissolved in $CDCl_3$ and filtered off into an NMR tube. NB: If not specified GB in Table 4, the introduction of the reagents and solvents into the microwave vial were performed under air.
Hot filtration test: 0.2 mol% of NiCl@RIO-12**e** and 3 mL of toluene were added to a microwave vial in the glovebox. The sealed vial was placed in the microwave oven and the mixture reacted for 15 minutes at 180°C. After that, the sealed tube was taken back into the glovebox, the catalyst NiCl@RIO-12**e** was filtered off the solution and the filtrate was transferred to a new vial. The reagents 4'-bromoacetophenone (1 equiv., 1 mmol, 0.203 g), phenylboronic acid (1.3 equiv.,1.3 mmol, 0.162 g) and tripotassium phosphate (2.6 equiv., 2.6 mmol, 0.563 g) were added to the filtrate, the vial was sealed, and the mixture reacted at 180°C for 15 min. The resulting mixture was analysed by $^1H$ NMR spectroscopy and only starting materials were detected.

## Acknowledgements

This study was financed in part by the Coordenação de Aperfeiçoamento de Pessoal de Nível Superior – Brasil (CAPES) – Finance Code 001; CAPES scholarship PDSE Process Number 88881.189512/2018-01, CNPq and FAPERJ. We thank Dr. Sangaraju Shanmugam (Daegu Gyeongbuk Institute of Science and Technology - DGIST) for performing the TEM-EDS analyses. VR thanks the Institut Universitaire de France for financial support.

**Keywords:** Covalent Organic Framework • Nickel • Heterogeneous Cross-Coupling • Microwave Heating

[1] A. P. Côté, A. I. Benin, N. W. Ockwig, M. O'Keeffe, A. J. Matzger, O. M. Yaghi, *Science* **2005**, *310*, 1166–1170.

[2] S. Y. Ding, J. Gao, Q. Wang, Y. Zhang, W. G. Song, C. Y. Su, W. Wang, *J. Am. Chem. Soc.* **2011**, *133*, 19816–19822.

[3] Z. J. Mu, X. Ding, Z. Y. Chen, B. H. Han, *ACS Appl. Mater. Interfaces* **2018**, *10*, 41350–41358.

[4] M. Zhang, R. Zheng, Y. Ma, R. Chen, X. Sun, X. Sun, *Microporous Mesoporous Mater.* **2019**, 285, 70–79.

[5] R. W. Tilford, W. R. Gemmill, H. C. Zur Loye, J. J. Lavigne, *Chem. Mater.* **2006**, *18*, 5296–5301.

[6] A. P. Côté, H. M. El-Kaderi, H. Furukawa, J. R. Hunt, O. M. Yaghi, *J. Am. Chem. Soc.* **2007**, *129*, 12914–12915.

[7] H. M. El-Kaderi, J. R. Hunt, J. L. Mendoza-Cortés, A. P. Côté, R. E. Taylor, M. O'Keeffe, O. M. Yaghi, *Science* **2007**, *316*, 268–272.

[8] R. A. Maia, F. L. Oliveira, M. Nazarkovsky, P. M. Esteves, *Cryst. Growth Des.* **2018**, *18*, 5682–5689.

[9] X. Feng, X. Ding, D. Jiang, *Chem. Soc. Rev.* **2012**, *41*, 6010-6022.

[10] S. Y. Ding, W. Wang, *Chem. Soc. Rev.* **2013**, *42*, 548–568.

[11] L. Deng, J. Zhang, Y. Gao, *Synthesis, Properties, and Their Potential Application of Covalent Organic Frameworks (COFs),* in *Mesoporous Mater. - Properties and Applications.* **2018**, InterchOpen.

[12] S. L. James, *Chem. Soc. Rev.* **2003**, *32*, 276–288.

[13] M. Safaei, M. M. Foroughi, N. Ebrahimpoor, S. Jahani, A. Omidi, M. Khatami, *TrAC - Trends Anal. Chem.* **2019**, *118*, 401–425.

[14] S. Ernst, *Angew. Chem. Int. Ed.* **2011**, *50*, 5425–5426.

[15] C. G. S. Lima, N. M. Moreira, M. W. Paixão, A. G. Corrêa, *Curr. Opin. Green Sustain. Chem.* **2019**, *15*, 7–12.

[16] Y. Han, M. Zhang, Y. Q. Zhang, Z. H. Zhang, *Green Chem.* **2018**, *20*, 4891–4900.

[17] H. Furukawa, O. M. Yaghi, *J. Am. Chem. Soc.* **2009**, *131*, 8875–8883.

[18] J. M. C. Cifuentes, B. X. Ferreira, P. M. Esteves, C. D. Buarque, *Top. Catal.* **2018**, *61*, 689–698.

[19] P. J. Waller, F. Gándara, O. M. Yaghi, *Acc. Chem. Res.* **2015**, *48*, 3053–3063.

[20] Z. Miao, G. Liu, Y. Cui, Z. Liu, J. Li, F. Han, Y. Liu, X. Sun, X. Gong, Y. Zhai, Y. Zhao, Y. Zeng, *Angew. Chem. Int. Ed.* **2019**, *58*, 4906–4910.

[21] J. Jiang, Y. Zhao, O. M. Yaghi, *J. Am. Chem. Soc.* **2016**, *138*, 3255–3265.

[22] H. Hu, Q. Yan, R. Gen, Y. Gao, *Chinese J. Catal.* **2018**, *39*, 1167–1179.

[23] W. Tu, Y. Xu, S. Yin, R. Xu, *Adv. Mater.* **2018**, *30*, 1707582.

[24] R. S. B. Gonçalves, A. B. V. de Oliveira, H. C. Sindra, B. S. Archanjo, M. E. Mendoza, L. S. A. Carneiro, C. D. Buarque, P. M. Esteves, *ChemCatChem* **2016**, *8*, 743–750.

[25] D. Cao, J. Lan, W. Wang, B. Smit, *Angew. Chem. - Int. Ed.* **2009**, *48*, 4730–4733.

[26] Z. Li, Y. Zhi, X. Feng, X. Ding, Y. Zou, X. Liu, Y. Mu, *Chem. - A Eur. J.* **2015**, *21*, 12079–12084.

[27] C. J. Doonan, D. J. Tranchemontagne, T. G. Glover, J. R. Hunt, O. M. Yaghi, *Nat. Chem.* **2010**, *2*, 235–238.

[28] C. Wang, Y. Wang, R. Ge, X. Song, X. Xing, Q. Jiang, H. Lu, C. Hao, X. Guo, Y. Gao, D. Jiang, *Chem. - A Eur. J.* **2018**, *24*, 585–589.

[29] A. K. Mandal, J. Mahmood, J. B. Baek, *ChemNanoMat* **2017**, *3*, 373–391.

[30] Y. Zhang, S. N. Riduan, J. Wang, *Chem. - A Eur. J.* **2017**, *23*, 16419.

[31] S. Wang, Q. Wang, P. Shao, Y. Han, X. Gao, L. Ma, S. Yuan, X. Ma, J. Zhou, X. Feng, B. Wang, *J. Am. Chem. Soc.* **2017**, *139*, 4258–4261.

[32] H. Ma, B. Liu, B. Li, L. Zhang, Y. G. Li, H. Q. Tan, H. Y. Zang, G. Zhu, *J. Am. Chem. Soc.* **2016**, *138*, 5897–5903.

[33] L. Bai, S. Z. F. Phua, W. Q. Lim, A. Jana, Z. Luo, H. P. Tham, L. Zhao, Q. Gao, Y. Zhao, *Chem. Commun.* **2016**, *52*, 4128–4131.

[34] Q. Fang, J. Wang, S. Gu, R. B. Kaspar, Z. Zhuang, J. Zheng, H. Guo, S. Qiu, Y. Yan, *J. Am. Chem. Soc.* **2015**, *137*, 8352–8355.

[35] Y. Luo, J. Liu, Y. Liu, Y. Lyu, *J. Polym. Sci. Part A Polym. Chem.* **2017**, *55*, 2594–2600.

[36] J. Romero, D. Rodriguez-San-Miguel, A. Ribera, R. Mas-Ballesté, T. F. Otero, I. Manet, F. Licio, G. Abellán, F. Zamora, E. Coronado, *J. Mater. Chem. A* **2017**, *5*, 4343–4351.

[37] H. Yang, L. Yang, H. Wang, Z. Xu, Y. Zhao, Y. Luo, N. Nasir, Y. Song, H. Wu, F. Pan, Z. Jiang, *Nat. Commun.* **2019**, *10*, 2101.

[38] B. P. Biswal, H. A. Vignolo-González, T. Banerjee, L. Grunenberg, G. Savasci, K. Gottschling, J. Nuss, C. Ochsenfeld, B. V. Lotsch, *J. Am. Chem. Soc.* **2019**, *141*, 11082–11092.

[39] R. Chen, J.-L. Shi, Y. Ma, G. Lin, X. Lang, C. Wang, *Angew. Chem. Int. Ed.* **2019**, *58*, 6430–6434.

[40] M. Bhadra, S. Kandambeth, M. K. Sahoo, M. Addicoat, E. Balaraman, R. Banerjee, *J. Am. Chem. Soc.* **2019**, *141*, 6152–6156.

[41] M. Mu, Y. Wang, Y. Qin, X. Yan, Y. Li, L. Chen, *ACS Appl. Mater. Interfaces* **2017**, *9*, 22856–22863.

[42] M. Zhao, C. De Wu, *Catal. Commun.* **2017**, *99*, 146–149.

[43] G. Singh, P. A. Singh, A. K. Sen, K. Singh, S. N. Dubey, R. N. Handa, J. Choi, *Synth. React. Inorg. Met. Chem.* **2002**, *32*, 171–187.

[44] S. A. Abdel-Latif, H. B. Hassib, Y. M. Issa, *Spectrochim. Acta Part A Mol. Biomol. Spectrosc.* **2007**, *67*, 950–957.

[45] F.-S. Han, *Chem. Soc. Rev.* **2013**, *42*, 5270.

[46] S. Z. Tasker, E. A. Standley, T. F. Jamison, *Nature* **2014**, *509*, 299–309.

[47] V. P. Ananikov, *ACS Catal.* **2015**, *5*, 1964–1971.

[48] M. Henrion, V. Ritleng, M. J. Chetcuti, *ACS Catal.* **2015**, *5*, 1283–1302.

[49] V. Ritleng, M. Henrion, M. J. Chetcuti, *ACS Catal.* **2016**, *6*, 890–906.

[50] C. Chen, L. M. Yang, *Tetrahedron Lett.* **2007**, *48*, 2427–2430.

[51] L. A. Baldwin, J. W. Crowe, D. A. Pyles, P. L. McGrier, *J. Am. Chem. Soc.* **2016**, *138*, 15134–15137.

[52] S. Nandi, S. K. Singh, D. Mullangi, R. Illathvalappil, L. George, C. P. Vinod, S. Kurungot, R. Vaidhyanathan, *Adv. Energy Mater.* **2016**, *6*, 1–11.

[53] H. Dong, X.-B. Meng, X. Zhang, H.L. Tang, J.-W. Liu, J.-H. Wang, J.-Z.-Wei, F.-M. Zhang, L.-L. Bai, X.-J. Sun, *Chem. Eng. J.* **2019**, *379*, 122342.

[54] M. Wang, X. Yuan, H. Li, L. Ren, Z. Sun, Y. Hou, W. Chu, *Catal. Commun.* **2015**, *58*, 154–157.

[55] L. Sibous, E. Bentouhami, A. Maïza, G. M. Bouet, M. A. Khan, *J. Solution Chem.* **2010**, *39*, 511–521.

[56] M. Dolaz, M. Tümer, M. Diğrak, *Transit. Met. Chem.* **2004**, *29*, 528–536.

[57] S. Damavandi, N. Samadieh, S. Ahmadjo, Z. Etemadinia, G. H. Zohuri, *Eur. Polym. J.* **2015**, *64*, 118–125.

[58] A. J. Howarth, A. W. Peters, N. A. Vermeulen, T. C. Wang, J. T. Hupp, O. K. Farha, *Chem. Mater.* **2017**, *29*, 26–39.

[59] C. Yawns, *Surface Tension - Organic Compounds,* in *Thermophysical Properties of Chemicals and Hydrocarbons*, William Andrew, **2008**, pp.689-780.

[60] E. Canpolat, M. Kaya, *J. Coord. Chem.* **2004**, *57*, 1217–1223.

[61] S. M. Ben-saber, A. A. Maihub, S. S. Hudere, M. M. El-ajaily, *Microchem. J.* **2005**, *81*, 191–194.

[62] J. Matienzo, L. I. Yin, S. O. Grim, W. E. Swartz, *Inorg. Chem.* **1973**, *12*, 2762–2769.

[63] A. Davidson, J. F. Tempere, M. Che, H. Roulet, G. Dufour, *J. Phys. Chem.* **1996**, *100*, 4919–4929.

[64] M. Nič, J. Jirát, B. Košata, A. Jenkins, A. McNaught, Eds., *IUPAC Compendium of Chemical Terminology*, IUPAC, Research Triagle Park, NC, **2009**.

[65] S. Karak, S. Kandambeth, B. P. Biswal, H. S. Sasmal, S. Kumar, P. Pachfule, R. Banerjee, *J. Am. Chem. Soc.* **2017**, *139*, 1856–1862.

[66] J. D. Bernal, *Proc. R. Soc. A Math. Phys. Eng. Sci.* **1924**, *106*, 749–773.

[67] O. Hassel, H. Mark, *Zeitschrift für Phys.* **1924**, *25*, 317–337.

[68] A. L. Patterson, *Phys. Rev.* **1939**, *56*, 978–982.

[69] A. M. Oertel, V. Ritleng, M. J. Chetcuti, *Organometallics* **2012**, *31*, 2829–2840.

[70] M. Baghbanzadeh, C. Pilger, C. O. Kappe, *J. Org. Chem.* **2011**, *76*, 1507–1510.

[71] R. Destro, A. Gavezzotti, M. Simonetta, *Acta Crystallogr. Sect. B Struct. Crystallogr. Cryst. Chem.* **1978**, *34*, 2867–2869.

## Entry for the Table of Contents

# FULL PAPER

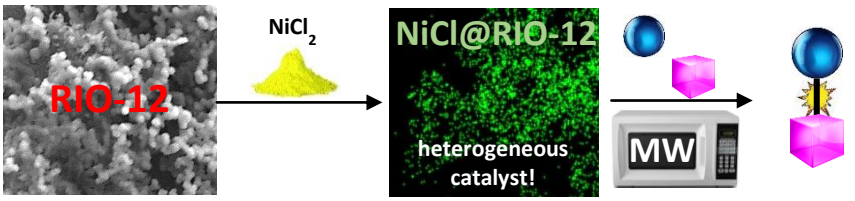


**Ni-Functionalized COF for Heterogeneous Catalysis:** Nickel-decorated COF materials NiCl@RIO-12 were synthetized with tuneable amount of nickel incorporation from 3.6 to 25 wt%. The paramagnetic material exhibited promising catalytic activity in Suzuki-Miyaura cross-coupling reactions under microwave heating. NiCl@RIO-12 demonstrated good thermal stability and its recyclability granted no substantial loss of activity upon 3 cycles.

*Renata A. Maia, Fabienne Berg, Vincent Ritleng,* Benoît Louis, Pierre M. Esteves**

***Page No. – Page No.***

**Design, Synthesis and Characterization of Nickel-Functionalized Covalent Organic Framework NiCl@RIO-12 for Suzuki-Miyaura Heterogeneous Catalysis**